DOI: 10.21791/IJEMS.2026.08

Research Paper

Sealing Performance of Beam Tube Flange Connections Under Internal Pressure and External Bending Loads

USMAN ASLAM[1], KAMRAN AHMED KHAN[2], WAQQAS AHMAD[3]

[1]Pakistan Institute of Engineering and Applied Sciences, Faculty of Engineering, Department of Mechanical Engineering, Pakistan. usmanaslam4720@gmail.com
[2]Pakistan Institute of Engineering and Applied Sciences, Faculty of Engineering, Department of Mechanical Engineering, Pakistan. drkamran@pieas.edu.pk (corresponding author)
[3]Pakistan Institute of Engineering and Applied Sciences, Faculty of Engineering, Department of Mechanical Engineering, Pakistan. waqqas@pieas.edu.pk

Received: 16 March 2026 **Accepted:** 13 May 2026 **Online Publication Date**: 13 May 2026

How to cite

U. Aslam, K.A. Khan, and W. Ahmad, "Sealing Performance of Beam Tube Flange Connections Under Internal Pressure and External Bending Loads", *International Journal of Engineering and Management Sciences*, pp. 1-19., May 2026 . doi: 10.21791/IJEMS.2026.08

Abstract. Pipe flange connections are critical components in nuclear and petrochemical facilities, where reliable sealing and structural integrity are essential for safe operation. In research on open-pool reactors, ion beam tubes represent a specialized application of flange-connected pressure boundaries. This study investigated the structural response and sealing performance of a beam tube–flange assembly using three-dimensional nonlinear finite element analysis. The beam tube was evaluated under two operating conditions: an empty configuration and a configuration subjected to externally applied mechanical loads. Stress analysis indicated that the maximum Von Mises stress in the beam tube remained well below the material yield strength and satisfied the design deformation limit of 3 mm for both loading scenarios. Sealing performance assessment of the flange joint showed a bolt stress variation of 23 MPa, which remained within acceptable design limits. The corresponding gasket stress variation was 0.49 MPa, with maximum and minimum gasket stresses were within the recommended operating range of 1.4–8 MPa. Time-dependent analysis revealed gasket stress relaxation of 3.5% for the empty beam tube and 3.78% for the externally loaded case. The finite element results were validated using analytical models, demonstrating good agreement with discrepancies ranging from 0.01% to 5.8%. The findings confirmed the structural adequacy and sealing reliability of the beam tube–flange assembly under the investigated operating conditions, providing a robust basis for safe design and operation in research reactor applications.

Keywords: Bolted Joints, FEA, TCM, SCM, EPDM, Stress Relaxation, Gasket Stress.

Introduction

Pipe flange connections are widely used in nuclear, industrial, and petrochemical engineering systems as reliable mechanical joints for connecting pipes, pumps, and auxiliary equipment. Their modularity, ease of installation, dismantling, maintenance, and inspection make them indispensable in safety-critical

DOI: 10.21791/IJEMS.2026.08

applications. From a mechanical engineering perspective, flange joints are complex assemblies in which structural integrity, load transfer, and sealing performance are strongly interdependent. Consequently, their behaviour under combined loading conditions remains an important subject of investigation.

A notable and specialized application of flange connections is found in ion-beam tube systems used in open-pool research reactors. In such facilities, ion beam tubes are used to irradiate material samples with neutrons for experimental and scientific studies. Structurally, a beam tube behaves as a cantilevered component: one end extends freely into the reactor pool, while the opposite end is rigidly supported by a structural boundary. At the supported end, the beam tube is connected to a sleeve embedded in the pool's concrete wall via a flange. This flange joint provides both mechanical restraint and a sealing barrier, preventing the release of radioactive media to the external environment. When subjected to external mechanical loads, the combined effects of structural stresses, joint deformation, and sealing response can significantly influence the performance and safety of the beam tube assembly. Therefore, understanding the mechanical and sealing behaviour of flange joints in such configurations is essential for ensuring long-term operational reliability.

Extensive research has been conducted on the sealing performance of flange joints, with much of the existing literature focusing on metallic gasketed connections. Various flange types are employed in industrial practice depending on application requirements, including weld neck, slip-on, threaded, and blind flanges. Among these, weld neck flanges are widely used in high-pressure and high-temperature applications due to their superior strength and favourable stress distribution characteristics [1]. Gaskets serve as the primary sealing elements in flange joints and are available in metallic, non-metallic, polymeric, and hybrid forms. Polymeric gaskets, such as Ethylene Propylene Diene Monomer (EPDM) and PTFE, are particularly attractive for nuclear applications owing to their corrosion resistance and thermal stability [2]. Gasket selection depends on several factors, including material compatibility, operating pressure and temperature, and service environment [3].

Design, assembly, and installation of flange joints are governed by established industrial standards. Organizations such as ASME, ANSI, and Garlock provide detailed guidelines covering flange dimensions, material specifications, bolt selection, gasket characteristics, and tightening procedures. For instance, ASME PCC-1 specifies recommended bolt tightening sequences and multi-pass tightening strategies, while ASME B16.5 defines flange dimensions, materials, and bolting requirements. Garlock guidelines provide gasket pressure–temperature ratings and recommended tightening torque [1, 3, 4].

Previous studies have examined several factors influencing flange joint performance. The relative importance of minimum gasket seating stress and flange rotation has been investigated, with findings suggesting that minimum seating stress may represent a more appropriate failure criterion than the flange rotation limits prescribed by ASME [5]. Traditional flange-joint design methods typically consider internal pressure as the primary load case; however, the influence of external bending moments has also been examined using finite-element analysis [6]. Iterative numerical approaches have been proposed to account for non-uniform bolt stresses and achieve more uniform gasket stress distributions [7]. The effects of thermal transient loading [8], external bending moments on single and twin gasket configurations [9], and different bolt tightening strategies, such as torque-controlled (TCM) and stretch-controlled methods (SCM), have been extensively studied, with optimized tightening procedures proposed to improve sealing performance [10-13]. Furthermore, significant effort has been devoted to

DOI: 10.21791/IJEMS.2026.08

modeling the material behaviour of EPDM gaskets, with hyperelastic and viscoelastic constitutive models calibrated and implemented by finite element analysis [14-22].

Despite these contributions, limited attention has been given to flange joint behaviour in beam tube assemblies where structural response and sealing performance must be simultaneously satisfied under reactor-specific loading conditions. In particular, studies integrating beam tube stress analysis, gasket sealing behaviour, and time-dependent material effects within a unified numerical framework remain scarce. In the present work, a three-dimensional nonlinear finite element analysis of a beam tube–flange assembly incorporating an EPDM gasket is performed. The study focuses on the stress response of the beam tube and the sealing performance of the flange joint under representative operating conditions, aiming to provide mechanically sound insights relevant to nuclear research reactor applications.

1. Materials and Methods

An overview of the methodology employed for the present study is presented in Figure 1.

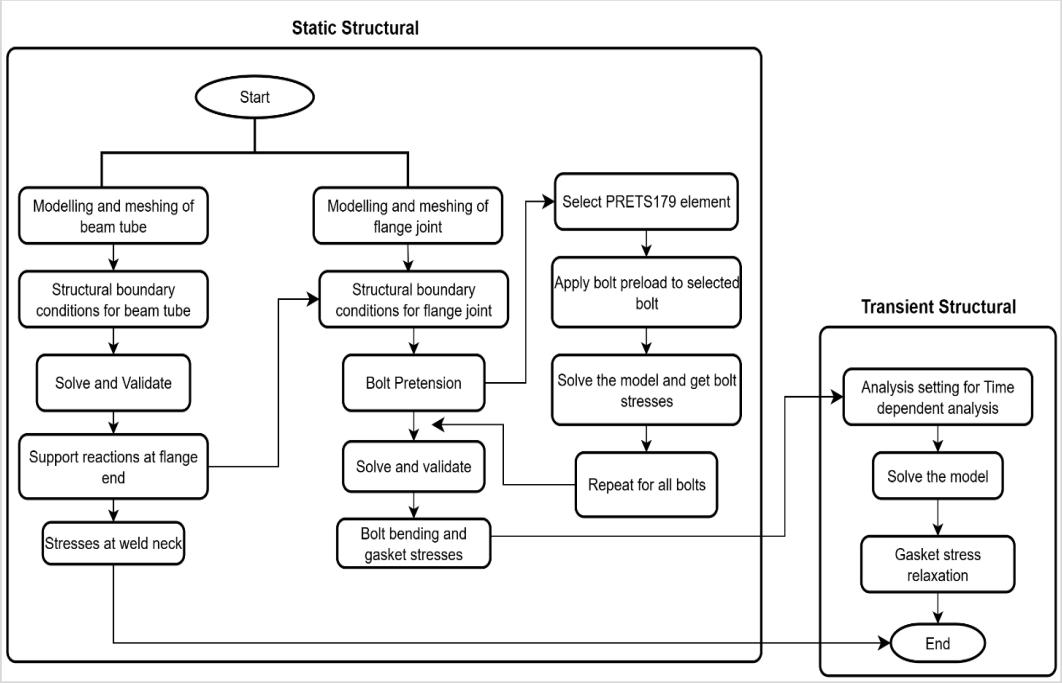

Figure 1. FEA Methodology

The analysis was divided into two primary sections: the second section covered time-dependent (transient) behavior, while the first covered steady-state analysis.

To determine the initial stress state, bolt preload, and gasket contact pressure immediately after assembly, which govern primary sealing performance, a steady-state analysis was conducted in the first section. For computational efficiency, this section was further divided into two parts, where the beam tube was modeled independently, followed by the flange joint assembly. Since the beam tube's response was essentially independent of the flange joint, the beam tube was examined separately to determine the stress distribution and support reactions at the flange interface. These reactions were then used as boundary conditions in the flange joint model, where gasket and bolt stresses were determined by evaluating bolt pretension and contact interactions. To evaluate stress relaxation and its effect on long-

DOI: 10.21791/IJEMS.2026.08

term sealing integrity, a transient analysis was carried out in the second section to account for the viscoelastic nature of the EPDM gasket.

1.1. Geometric Modeling

A general-purpose finite element analysis software [23] was used to construct an axisymmetric model of a beam tube, which was then revolved to produce a full three-dimensional model. An independent three-dimensional flange joint model was created. The flange had two faces: one was part of the beam tube, and the other was part of the sleeve that was embedded in the open pool reactor's concrete wall. The geometrical dimensions of the beam tube flange joint assembly are provided in Table 1 . CAD models of the beam tube and flange joint are presented in

Figure 2, Figure 3, Figure 4, and Figure 5.

Geometric Parameters	Symbol	Value
Flange (sleeve face) diameter	D	430mm
Flange (beam tube face) diameter	D1	385mm
Beam tube diameter	D2	254mm
Beam tube step diameter	D3	200mm
Beam tube thickness	t	8mm
Flange sleeve face thickness	t1	40mm
Flange Beam tube face thickness	t2	15mm
Gasket thickness	t3	5mm
Number of studs and bolts	N	12
Stud pitch circle diameter	D_P	240mm
Length of step	L1	968mm
Length of step	L2	2500mm

Table 1. Geometrical dimensions of flange joint assembly

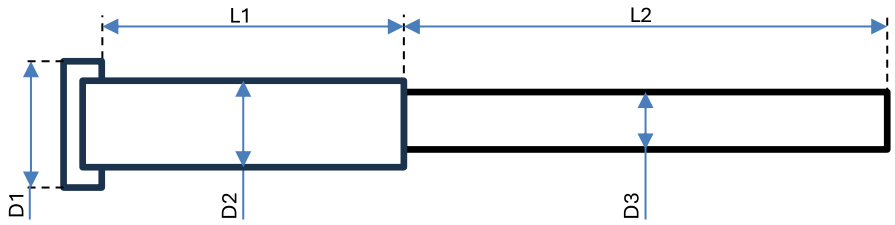

Figure 2. Schematic of beam tube flange assembly

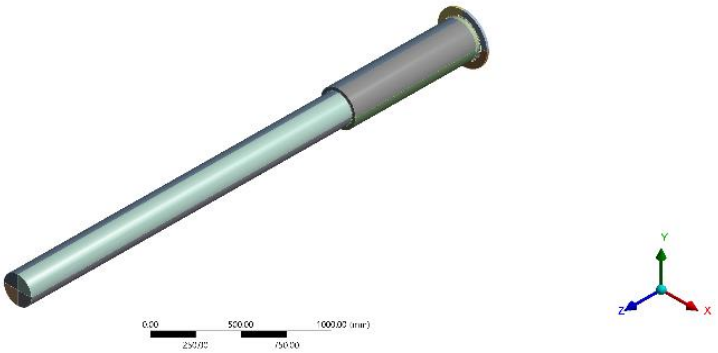

Figure 3. CAD model of beam tube

DOI: 10.21791/IJEMS.2026.08

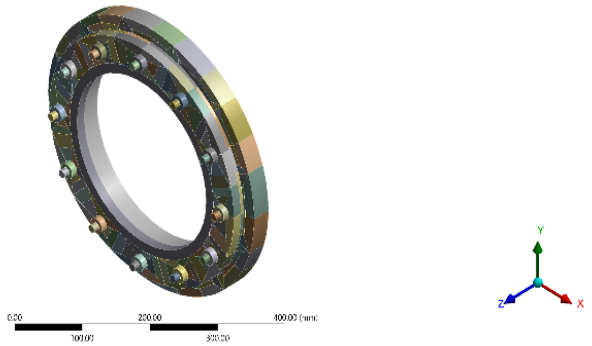

Figure 4. CAD model of flange joint

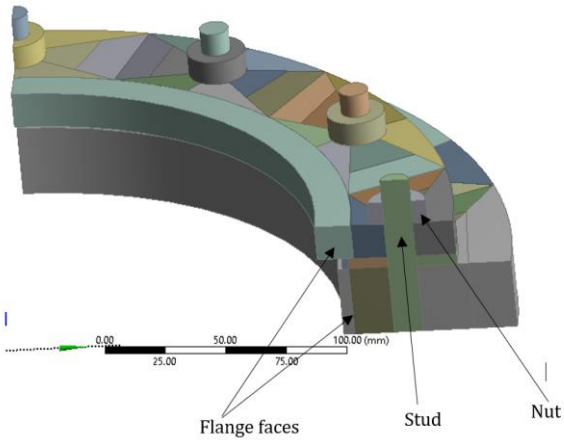

Figure 5. Sectional view of bolted flange joint

1.2. Material Selection

The beam tube and one face of the flange were manufactured from aluminium alloy 6061-O, which offers a high strength-to-weight ratio and corrosion resistance. Fasteners were made from SA 479 316, and the gasket was of EPDM material.

1.3. Material Models

All components of the flange assembly were modeled using a linear isotropic elasticity model, except the EPDM gasket. Material properties of components are presented in Table 2. EPDM rubber was modeled with a hyperelastic-viscoelastic material model, which is a combination of the Prony shear relaxation model and the Neo-Hookean model, shown in Tables 3 and 4.

Materials	**Density (kgm^{-3})**	**Poisson ratio**	**Allowable stress (MPa)**	**Youngs Modulus (GPa)**
Flange (Tube side) Aluminum 6061-O	2700	0.33	131	68
Flange (Sleeve side) SA 240 316	8027	0.30	310	193
Nuts and Bolts SA 479 316	8000	0.30	450	193

Table 2. Material properties of assembly components [24]

DOI: 10.21791/IJEMS.2026.08

J	1	2	3	4
g_j	0.08	0.08	0.06	0.02
τ_j(s)	2.09	13.03	117.80	349.87

Table 3. Time-dependent model parameters of EPDM [25]

Initial Shear Modulus (MPa)	μ	22.5
Incompressibility Parameter (MPa^{-1})	D	0

Table 4. Hyperelastic model parameters of EPDM

1.4. Meshing

The beam tube and flange joint were sliced to obtain a structured hexahedral mesh. Mesh refinement was performed on filleted regions of the beam tube to capture stress concentrations. The component meshing is shown in Figure 6.

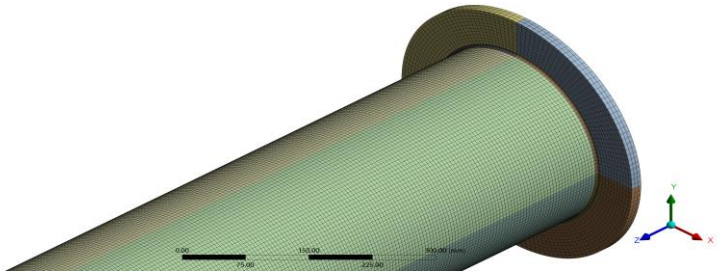

(a)

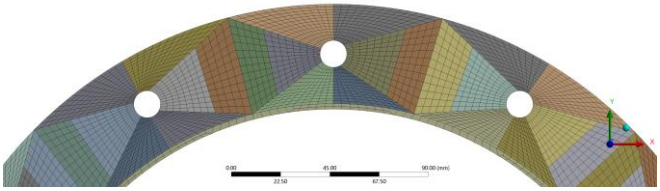

(b)

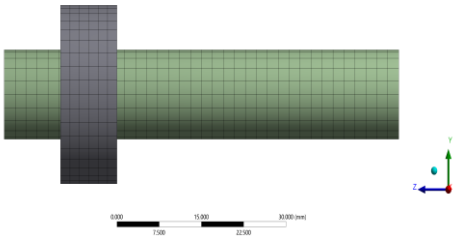

(c)

Figure 6. Meshing (a) beam tube (b) gasket (c) Stud and nut

1.5. Contacts

To ensure proper interaction, four connections were defined between the various flange joint components. The outer face of the stud and the inner face of the nut formed a bonded contact. The nut face and the flange face had a frictional contact with a coefficient of friction of 0.2. Between the gasket faces and the matching flange faces, there were two frictional contacts with a coefficient of friction of

DOI: 10.21791/IJEMS.2026.08

0.3. The beam tube and flanges were modeled using the SOLID186 element. Contacts between matching surfaces were made using CONTA174 and TARGE170.

1.6. Boundary Conditions

The beam tube flange assembly was analysed in two sequential sections. In the first section, a detailed stress analysis of the beam tube was performed. The resulting bending moment at the flange sleeve face, together with the internal pressure, was subsequently applied as loading conditions to the flange joint model in the second section. Two loading cases were considered for the beam tube stress analysis. In the first case, referred to as the empty beam tube, the structure was subjected to a hydrostatic pressure of 0.09 MPa, a fixed support at one end to represent the flange sleeve face, and gravitational loading. The second case, termed the standby beam tube, included additional loads due to concrete plugs and the weight of water within the beam tube, along with the boundary conditions defined in the empty beam tube case. Boundary conditions for the empty and standby beam tube cases are presented in Figure 7.

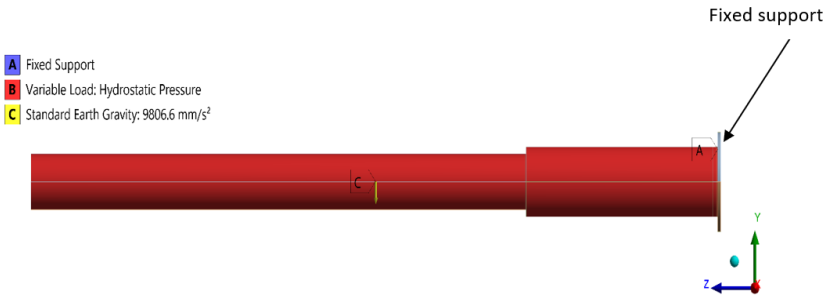

(a)

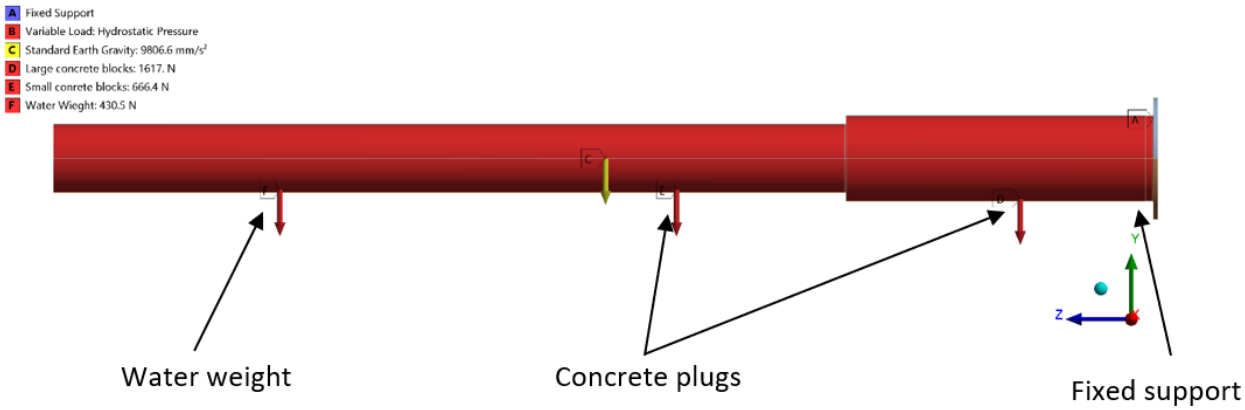

(b)

Figure 7. Boundary conditions of beam tube (a) Empty case (b) Standby case

Support reactions from the beam tube, i.e., bending moment, along with internal pressure of 0.09 MPa, were applied on the flange joint as boundary conditions. A fixed support was provided at the outer face of the sleeve side of the flange joint to depict the real-world behaviour of the assembly. The boundary conditions of the flange joint are shown in Figure 8.

DOI: 10.21791/IJEMS.2026.08

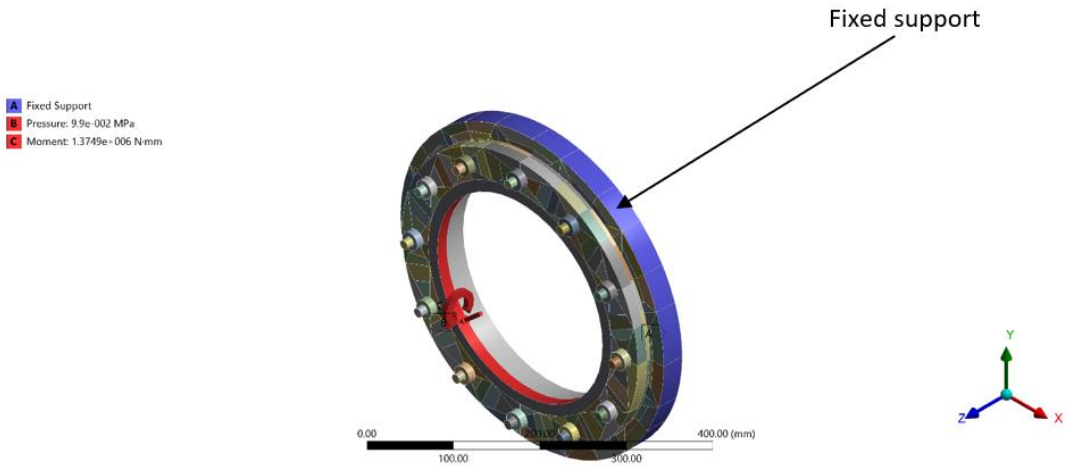

Figure 8. Boundary conditions of the flange joint

1.7. Bolt Preloading

Bolt preloading was performed in accordance with ASME PCC regulations and the torque-control method. Usually, bolt pretensions were applied iteratively by applying displacement (Uy) to the bottom face of the bolt or stud; however, in this study, bolt pretension was applied using the PRETS179 bolt element from ANSYS Mechanical. Bolt pretensions were created by directly applying the ASME-recommended bolt preload. This approach enabled us to achieve the required stress in a substantially reduced computing time. Target stress and bolt pretension for each pass are displayed in Table 5.

Target Torque	**Bolt stress for each pass (MPa)**			
59.2 Nm	Pass-1	Pass-2	Pass-3	Pass-4
% Of target load	30%	70%	100%	100%
Torque (Nm)	17.76	41.5	59.2	59.2
Load (kN)	5.92	13.81	19.73	19.73
Stress (MPa)	70.2	163.8	234	234
Sequence	1	1	1	2

Table 5. Bolt torque as per ASME PCC [26]

In the first three passes, Sequence -1 was (1-7-4-10-2-8-5-11-3-9-6-12), and in the last pass, (1-2-3-4-5-6-7-8-9-10-11-12) was followed. The Sequence of studs is given in Figure 9.

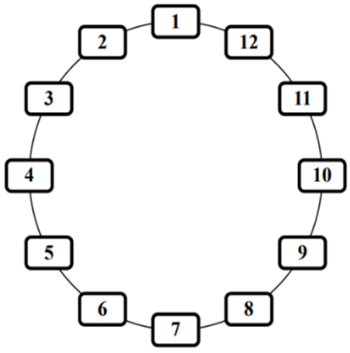

Figure 9. Bolts Numbering

DOI: 10.21791/IJEMS.2026.08

1.8. Analysis Settings in Finite Element Model

1.8.1. Static Structural Analysis

The nonlinear analysis of the flange joint was performed with 50 time steps. In the first step, a small preload of 100N was applied to stabilize the model. Bolt pretensioning was then carried out in the next 48 steps for 12 studs in four sequential passes, following the recommended tightening procedure. In the final (50th) step, operational loads from the beam tube were applied to the flange. The solver settings included program-controlled solver type and pivot checking, with weak springs and inertia relief turned off. To take geometric nonlinearity into consideration, large deflection was turned on, ensuring accurate simulation of contact behaviour and deformation during bolt tightening and load application. Figure 10 presents the analysis settings for steady-state analysis.

Details of "Analysis Settings"	
Step Controls	
Number Of Steps	50.
Current Step Number	1.
Step End Time	1. s
Auto Time Stepping	Program Controlled
Solver Controls	
Solver Type	Program Controlled
Weak Springs	Off
Solver Pivot Checking	Program Controlled
Large Deflection	On
Inertia Relief	Off

Figure 10. Analysis settings for steady-state analysis

1.8.2. Transient Structural Analysis

To capture the nonlinear behaviour during bolt tightening and loading, a total of 51 time steps were used in the transient analysis. The first 50 steps, which represented the initial tightening of 100N, a four-pass bolt pretensioning operation for all 12 bolts, and loading application, were in the same order as the static structural analysis. To depict the assembly's time-dependent response, the last (51st) step set the simulation's overall duration to 40,000 seconds. To guarantee steady convergence, auto time stepping was turned on with an initial and minimum time step of 0.2 seconds and a maximum of 500 seconds. The solver type was program-controlled, weak springs were disabled, and large deflection was turned on to accommodate geometric nonlinearities. Figure 11 presents settings implemented for time-dependent analysis.

Details of "Analysis Settings"	
Step Controls	
Number Of Steps	51.
Current Step Number	51.
Step End Time	40000 s
Auto Time Stepping	On
Define By	Time
Carry Over Time Step	Off
Initial Time Step	0.2 s
Minimum Time Step	0.2 s
Maximum Time Step	500. s
Time Integration	On
Solver Controls	
Solver Type	Program Controlled
Weak Springs	Off
Large Deflection	On

Figure 11. Analysis settings for transient analysis

DOI: 10.21791/IJEMS.2026.08

2. Results and Discussions

Beam tube results are presented in two sections, followed by flange joint results using finite element analysis.

2.1. Empty Beam Tube Case

- Due to the self-weight of the beam tube and internal hydrostatic pressure, the maximum von Mises stress of 19.61 MPa occurred on the top surface of the welded region at the step on the beam tube, which was well within the yield limit of 131 MPa.
- Beam tube's free-end was deflected +1.6152 mm in the Y-direction, which was well within the design limit of 3 mm deformation.
- The calculated maximum deformation occurred at the free-end of the beam tube, which extruded freely in the reactor pool, as shown in Figure 12. The deformation within the beam tube section enclosed by the sleeve, which had an allowable deformation limit of 3 mm, was significantly lower, at less than 0.1 mm.

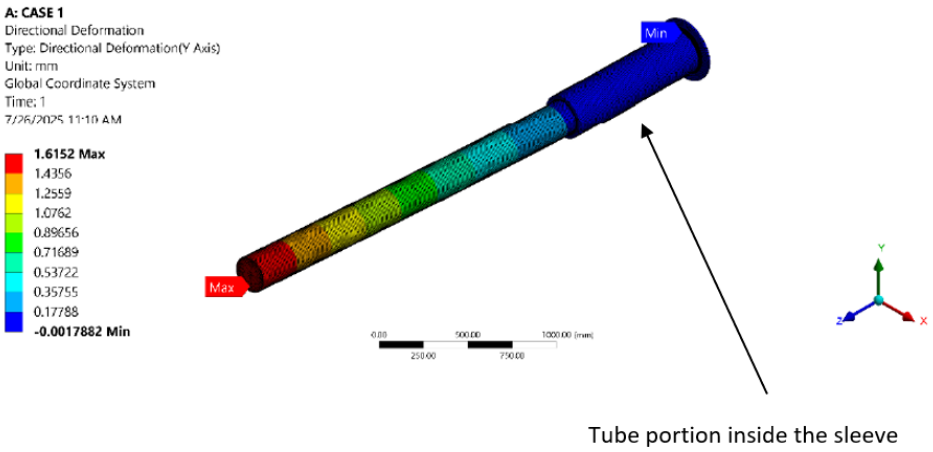

Figure 12. Directional deformation in the vertical direction for the empty case

Table 6 summarizes the stress analysis for the empty beam tube case, highlighting the maximum von Mises stress, the maximum directional deformation, and the support reactions at the fixed end.

Parameters	Value
Max Equivalent stress	19.616MPa
Max directional deformation (Y axis)	1.6152mm
Moment reaction	1374.9Nm
Normal reaction	5948.5N
Shear reaction	-888.86N

Table 6. Results of the Empty beam tube case

2.2. Standby Beam Tube Case

- Due to the self-weight of the beam tube, internal hydrostatic pressure, and external loads of concrete blocks and water, a maximum von Mises stress of 15.17 MPa occurred on the bottom surface of the welded region at the step on the beam tube, which was well within the yield limit of 131 MPa.

DOI: 10.21791/IJEMS.2026.08

- Beam tube was deflected downwards, and its free-end was deflected -1.1916 mm in the y-direction, which was well within the design limit of 3 mm deformation.
- The calculated maximum deformation occurred at the free-end of the beam tube, which extruded freely in reactor pool, and as shown in Figure 13, the deformation in the span, which was actually surrounded by a sleeve where the design deformation limit was 3 mm, was less than 0.1mm, while the maximum deformation at the free-end was -1.19mm in the Y-direction.

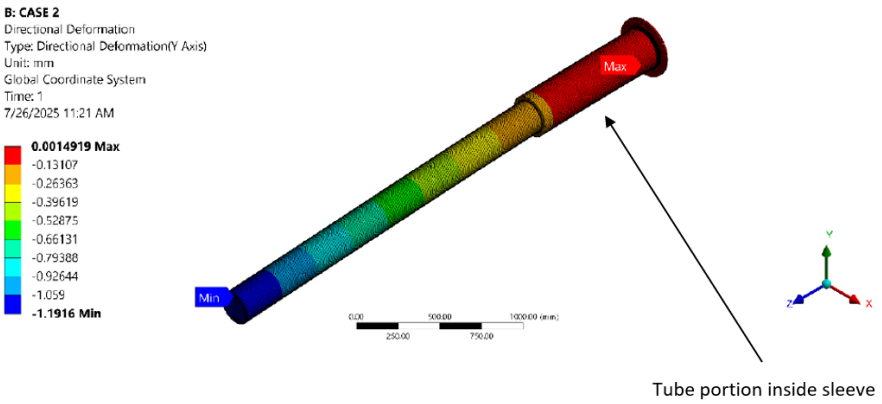

Figure 13. Directional deformation in the vertical direction for the standby case

Table 7 summarizes the stress analysis results for the standby beam tube.

Parameters	Value
Max Equivalent stress	15.175MPa
Min directional deformation (Y axis)	-1.1916mm
Moment reaction	-1489.4Nm
Normal reaction	5948.3N
Shear reaction	1824.9N

Table 7. Results of the Standby beam tube case

2.3. Analytical Solution for the Support Reactions of Beam Tube

An analytical model was prepared to calculate support reactions at the beam tube, and the results are presented in Table 8. The results showed very good agreement with the analytical results, with an error of less than 2%, indicating high accuracy of the FEA model.

	Empty beam tube case			Standby beam tube case		
Parameters	**FEA**	**Analytical**	**Error (%)**	**FEA**	**Analytical**	**Error (%)**
Moment Reaction (Nm)	1374.9	1391.13	1.1	1489.4	1513.86	1.6
Shear Reaction (N)	888.86	889.474	0.07	1824.9	1824	0.05
Normal Reaction (N)	5948.5	5947.62	0.014	5948.3	5947.6	0.011

Table 8. Comparison of Analytical and Numerical results

2.4. Flange Joint

This section presents a comprehensive analysis of the flange joint, exploring bolt stresses, bolt bending, gasket stress variation, and gasket stress relaxation.

DOI: 10.21791/IJEMS.2026.08

2.4.1. Axial Bolt Stress Variation

Figure 14 presents the variation in bolt equivalent stress after each tightening pass and load application. Initial tightening of bolts resulted in uneven stress distribution due to bolt scattering, which occurred as a result of elastic interactions between components of the flange assembly during sequential bolt tightening. After pass 1, a stress variation of 27 MPa was observed. At the end of pass-4, the stress variation reduced to 23 MPa, with the highest stress of 230.8 MPa on stud 12 and the lowest of 208 MPa on stud 1. After applying external loads in both cases, stress variation was observed: some studs relaxed, while others showed higher stress after the applied load. Overall, all the stress values remained inside the design limit.

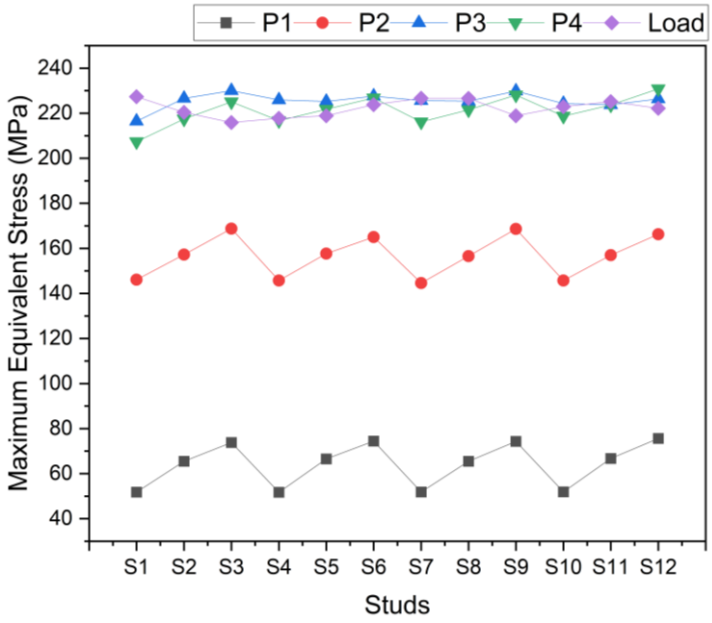

Figure 14. Stud stress variation during tightening passes

2.4.2. Bolt Bending

Four nodes, spaced at 90° intervals, were selected along the shank of each bolt to evaluate the bending behaviour of the studs. S1/N1 represented the inner node of Stud 1, located toward the inner periphery of the flange joint, while S1/N2 corresponded to the outer node positioned toward the outer periphery. The remaining nodes, S1/N3 and S1/N4, represented the lateral positions on the stud. The four nodes selected for Stud-1 are shown in Figure 15. In the same way, four nodes were selected for all twelve bolts, and the nodes were named based on the number of bolts and on the location of the node. The nodes selected for all twelve bolts with their nomenclature. Axial stresses for all the nodes were plotted against the tightening pass.

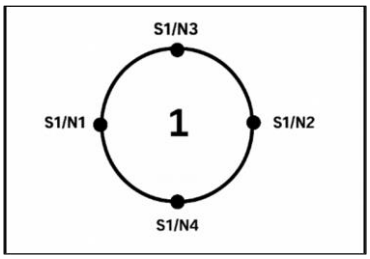

Figure 15. Nodes on the shank of stud 1

DOI: 10.21791/IJEMS.2026.08

Figure 16 and Figure 17 depict the stress distribution on four different nodes on each stud. Stress levels were displayed on the Y-axis of the graph, while loading passes were displayed on the X-axis. The graph showed that stress levels for every node in every stud increased steadily as the preload rose with every tightening pass.

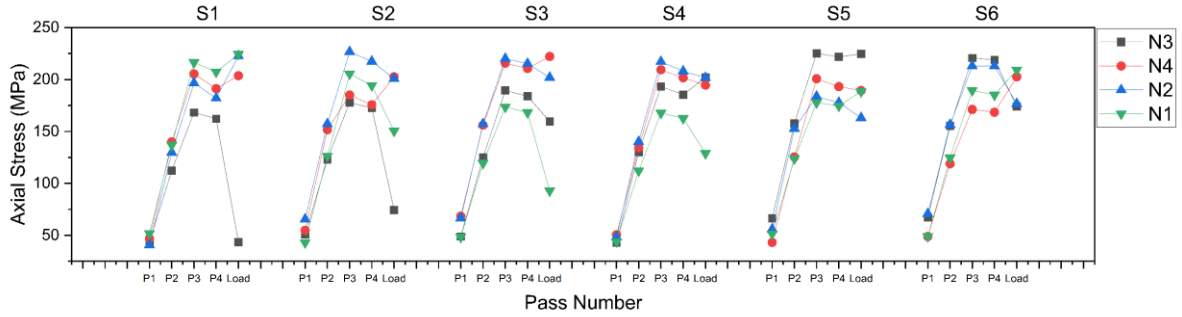

Figure 16. Bolt bending for stud 1-6

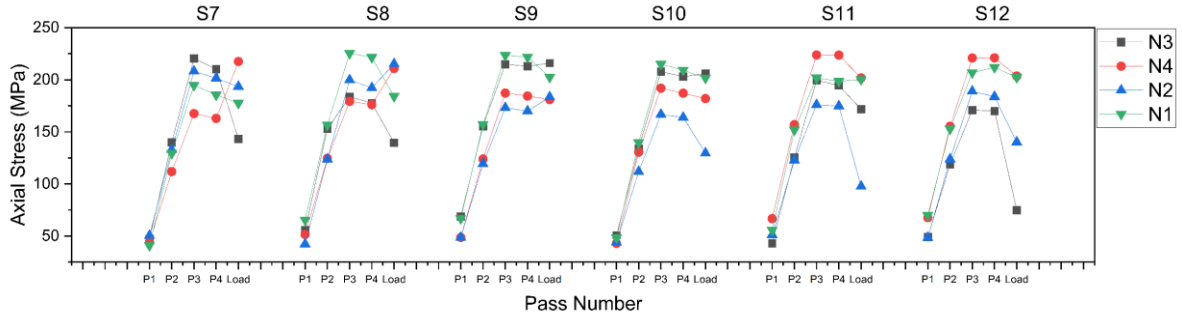

Figure 17. Bolt bending for stud 7-12

After applying load, most nodes decreased in stress, but some, possibly due to extreme joint bending, increased in stress. Due to severe loading and bending of the flange, one specific node at the flange joint's inner edge experienced the greatest stress. The graphs exhibit some variation due to bolt relaxation after the load was applied, even though they depict a general behavior of stud bending, with stress levels rising with each pass. Even though stress levels steadily increased with each pass, they remained within acceptable bounds, ensuring a secure and reliable flange junction.

2.4.3. Gasket Stress Variation

To study stress variation on the gasket, twelve nodes were selected at the innermost region of the gasket, an area mostly exposed to fluid, and twelve nodes at the outermost diameter of the gasket. Inner nodes were represented with (GI), while outer nodes were represented by (GO). Figure 18 shows the node selection on the gasket.

Figure 19 shows stress variation at different nodes, including inner and outer nodes. The X-axis of the graph represented the inner 12 nodes and the outer 12 nodes, while the Y-axis of the graph represented the normal stress values. Stress values at each node were presented at four passes, including after load application.

DOI: 10.21791/IJEMS.2026.08

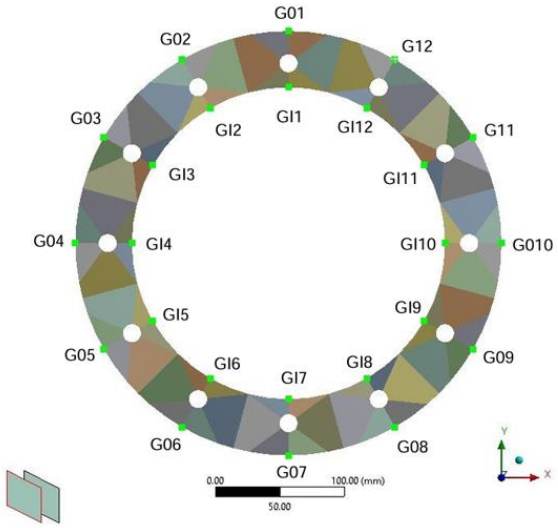

Figure 18. Nodes on the inner and outer diameters of the gasket

Because the inner nodes of the gasket were more exposed to fluid pressure and external loads, it was evident that the inner nodes (GI) experienced lower compressive stress than the outer nodes (GO). Following the fourth pass, Node 3's outer node stress value was the highest at -2.165 MPa, while Node 7's was the lowest at -1.663 MPa. Likewise, after the fourth pass, the inner node's maximum stress was -2.44 MPa on Node 9, while its minimum was -1.7354 MPa on Node 1.

Overall trends showed a general pattern of increasing stress levels for both inner and outside nodes after each loading run. Analysis clearly showed that while the outer nodes of the gaskets were well within the design limits, the interior nodes were more prone to leak because of less compressive stress. Overall, no leak or crushing was observed in the gasket.

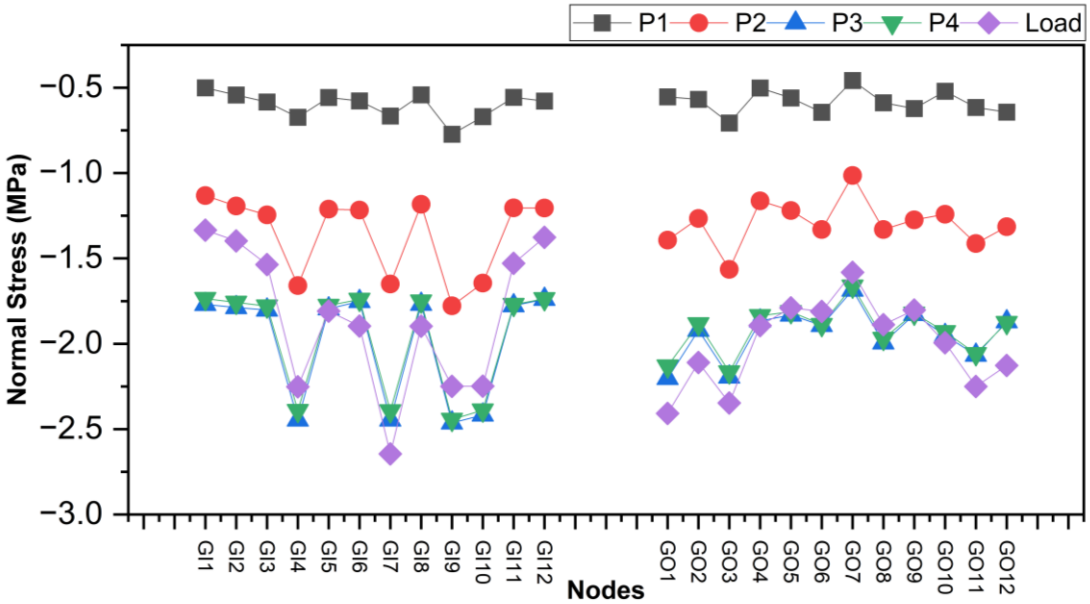

Figure 19. Gasket stress variation during loading

DOI: 10.21791/IJEMS.2026.08

The recommended minimum and maximum stress for elastomeric gaskets were 1.4 MPa and 8 MPa, respectively. Figure 20 shows that the minimum and maximum stresses were within the predefined stress range.

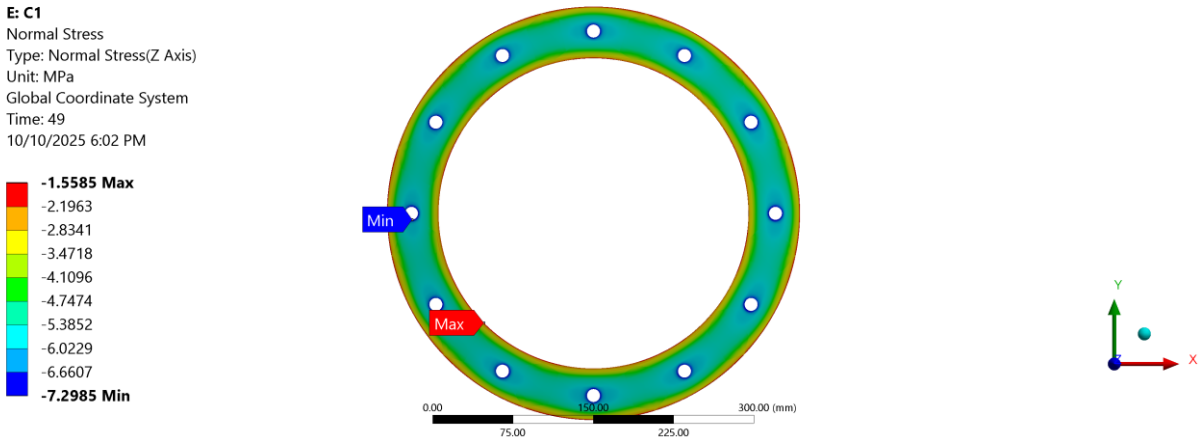

Figure 20. Gasket stress contour after joint assembly

To study gasket stress relaxation due to the viscoelastic behaviour of the EPDM gasket, time-dependent analysis was performed using transient structural analysis. Figure 21 represents the flange stress distribution 10 hours after joint assembly. The maximum equivalent stress on the flange was 97.46 MPa, well below the yield strength of 131 MPa, ensuring a safe flange joint.

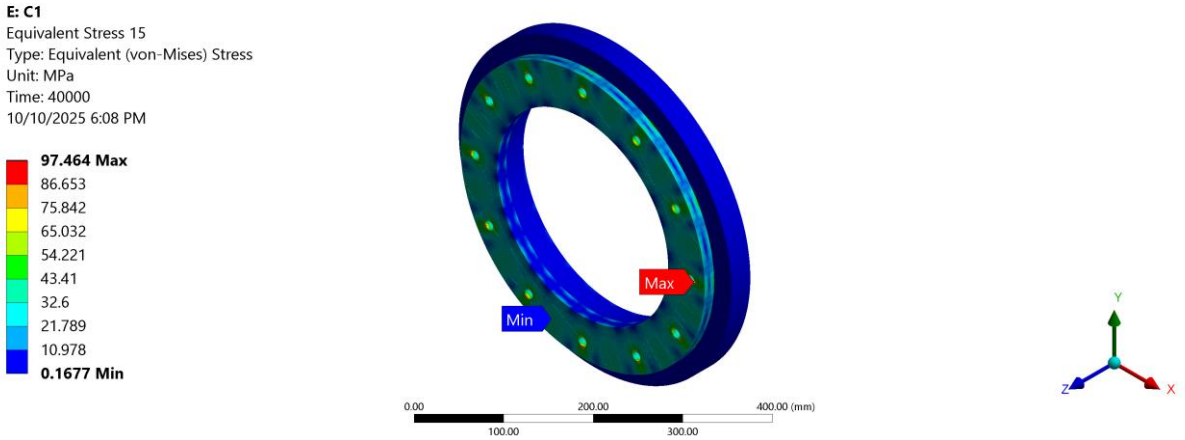

Figure 21. Flange stress contour after 10 hours of assembly

For both cases, after almost 35 minutes, the gasket stress reached a steady state. There was a decrease of 3.5% in stress value for case 1 and a 3.78% decrease for case 2, as shown in Figure 22. However, the maximum and minimum stress values were within an acceptable range of 1.4-8 MPa, thus ensuring the safe design of the flange joint immediately after assembly.

DOI: 10.21791/IJEMS.2026.08

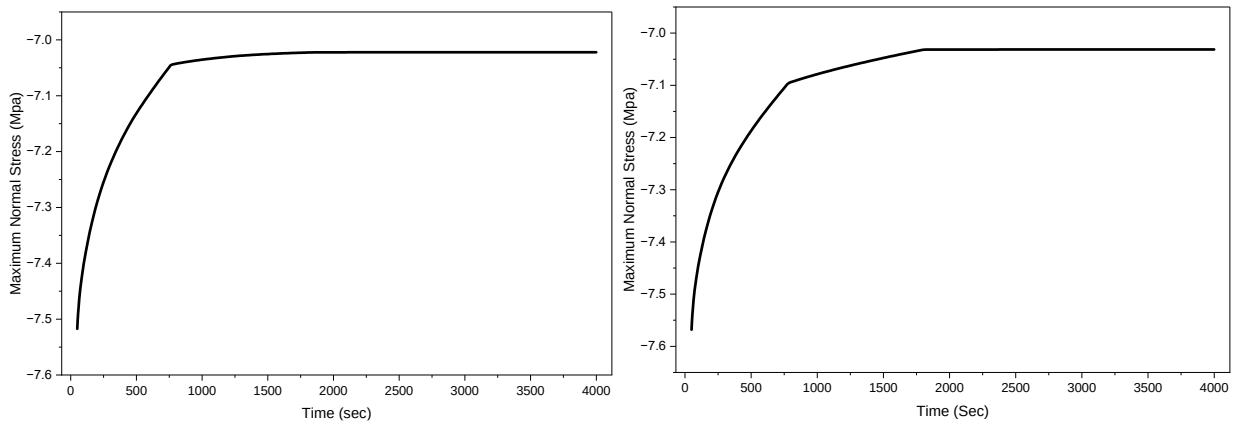

(a) (b)

Figure 22. Gasket stress relaxation (a) Empty beam tube case (b) Standby beam tube case

2.4.4. Validation of Results

According to the analytical model [23] that was constituted using the hyperelastic and viscoelastic models, fundamental equations were used to validate flange joint results. FEA results were in good agreement with the analytical results, as shown in Table 9, thereby confirming the FEA model's accuracy.

Parameters	FEA	Analytical	Error (%)
Initial Bolt stress (MPa)	221.2	234	5.4
Bolt stress after pressure applied (MPa)	221	232	4.7
Gasket compression (mm)	0.35	0.335	4.3
Gasket average contact stress after bolting (MPa)	4.428	4.704	5.8

Table 9. Comparison of analytical and numerical results

Conclusions

The following were the key conclusions from this study:

- In the case of the empty beam tube, the maximum von Mises stress was 19.6 MPa, and in the case of the standby beam tube, the maximum von Mises stress was 15.1 MPa, which were far below the yield strength of the material, i.e.,131 MPa, thus ensuring safe operations.
- Bolt tightening methods played an important role in flange structural stability. A bolt stress variation of 23 MPa was observed at the end of the final pass during bolting.
- In addition to achieving up to 98% of the target stress, using bolt elements for bolt preloading rather than an iterative technique saved a significant amount of computing time by allowing for only one simulation rather than numerous simulations.
- To evaluate the stud's bending behavior, the distribution of stress at four nodes on each stud was noted. The study found that stress levels increased gradually as tightening passes were applied, with some nodes bearing more strain than others, suggesting that the studs bent, although the stress levels remained within reasonable limits.
- The results showed that the gasket stress levels were within the recommended ranges for both crushing and seating stress, ensuring reliable sealing performance.

DOI: 10.21791/IJEMS.2026.08

- This study offered significant new information about the sealing behavior and structural integrity of beam tube flange assemblies under combined loading conditions. The results showed that the configuration under analysis offered sufficient structural strength and dependable sealing performance for use in nuclear research reactors. Furthermore, in safety-critical engineering systems, the established numerical framework can be a helpful tool for the design and optimization of bolted flange joints using polymeric gaskets.

Author Contributions

Usman Aslam: Literature Review, Writing, Software analysis, Data interpretation, Methodology; Kamran Ahmed Khan: Project administration, Supervision, Data interpretation; Waqqas Ahmad: Co-supervision, Data interpretation.

Acknowledgement

The authors gratefully acknowledge the support of the Project Director and his team, particularly Engr. Usman Maqbool, for facilitating access to the beam tube flange facility and enabling the conduct of this research.

Conflicts of Interest

The authors declare no conflict of interest.

References

[1] *ASME B16.5-2020*, A. S. o. M. Engineers, 2020.

[2] N. Aibada, R. Manickam, K. K. Gupta, and P. Raichurkar, "Review on various gaskets based on the materials, their characteristics and applications," *Int. J. Text. Eng. Process,* vol. 3, no. 1, pp. 12-18, 2017.

[3] *Garlock Fluid Sealing Products Technical Manual*, 2017.

[4] *ASME PCC-1*, A. S. o. M. Engineers, 2019.

[5] M. M. Krishna, M. Shunmugam, and N. S. Prasad, "A study on the sealing performance of bolted flange joints with gaskets using finite element analysis," *International Journal of Pressure Vessels and Piping,* vol. 84, no. 6, pp. 349-357, 2007.

[6] G. Mathan and N. S. Prasad, "A study on the sealing performance of flange joints with gaskets under external bending using finite-element analysis," *Proceedings of the Institution of Mechanical Engineers, Part E: Journal of Process Mechanical Engineering,* vol. 222, no. 1, pp. 21-29, 2008.

[7] I. Coria, I. Martín, A.-H. Bouzid, I. Heras, and M. Abasolo, "Efficient assembly of bolted joints under external loads using numerical FEM," *International Journal of Mechanical Sciences,* vol. 142, pp. 575-582, 2018.

DOI: 10.21791/IJEMS.2026.08

[8] K. Khan and I. Ahmed, "Combined loading performance analysis of gasketed bolted flange joints with emphasis on bolt scattering," *Journal of Mechanical Engineering and Sciences,* pp. 9564-9575, 2023.

[9] N. Rino Nelson, N. Siva Prasad, and A. Sekhar, "A study on the behavior of single-and twin-gasketed flange joint under external bending load," *Journal of Pressure Vessel Technology,* vol. 139, no. 5, p. 051204, 2017.

[10] *Bolt Tightning Handbook*, 2001.

[11] M. Abid, A. Khan, M. Hussain, and H. A. Wajid, "Optimized bolt tightening procedure for different tightening strategies—FEA study," *Proceedings of the Institution of Mechanical Engineers, Part E: Journal of Process Mechanical Engineering,* vol. 231, no. 2, pp. 236-249, 2017, doi: 10.1177/0954408915589687.

[12] M. Abid, A. Khan, D. H. Nash, M. Hussain, and H. A. Wajid, "Optimized bolt tightening strategies for gasketed flanged pipe joints of different sizes," *International Journal of Pressure Vessels and Piping,* vol. 139, pp. 22-27, 2016.

[13] M. Abid and Y. M. Khan, "The effect of bolt tightening methods and sequence on the performance of gasketed bolted flange joint assembly," *Structural Engineering and Mechanics,* vol. 46, no. 6, pp. 843-852, 2013.

[14] B. Fazekas and T. J. Goda, "Constitutive modelling of rubbers: Mullins effect, residual strain, time-temperature dependence," *International Journal of Mechanical Sciences,* vol. 210, p. 106735, 2021.

[15] D. Foltuț, E. Vălean, G.-I. Șoșoi, D.-T. Pascal, J. Pospisil, and M. Buzdugan, "Comprehensive Study of EPDM Rubber Properties: Temperature-Dependent Stiffness, Tensile Behavior and FEA Calibration," in *IOP Conference Series: Materials Science and Engineering*, 2024, vol. 1319, no. 1: IOP Publishing, p. 012025.

[16] C. Gong, C. Xie, H. Zhu, W. Ding, J. Song, and Y. Ge, "Time-varying compressive properties and constitutive model of EPDM rubber materials for tunnel gasketed joint," *Construction and Building Materials,* vol. 433, p. 136734, 2024.

[17] D. Huri and T. Mankovits, "Comparison of the material models in rubber finite element analysis," in *IOP Conference Series: Materials Science and Engineering*, 2018, vol. 393, no. 1: IOP Publishing, p. 012018.

[18] Z. Lei and Z. Wang, "Analysis of stress relaxation characteristics of rubber sealing gaskets under the influence of random parameters," *Iranian Journal of Science and Technology, Transactions of Mechanical Engineering,* vol. 45, no. 3, pp. 711-718, 2021.

[19] X. Liu, C. Liu, D. Zhu, and J. Lin, "A visco-hyperelastic constitutive model to characterize the stress-softening behavior of ethylene propylene diene monomer rubber," *Polymers,* vol. 15, no. 16, p. 3388, 2023.

[20] Y. Liu *et al.*, "Compressive stress-hydrothermal aging behavior and constitutive model of shield tunnel EPDM rubber material," *Construction and Building Materials,* vol. 320, p. 126298, 2022.

DOI: 10.21791/IJEMS.2026.08

[21] K. Sukcharoen, N. Noraphaiphipaksa, A. Hasap, and C. Kanchanomai, "Experimental and numerical evaluations of localized stress relaxation for vulcanized rubber," *Polymers,* vol. 14, no. 5, p. 873, 2022.

[22] X. Wang, Z. Wang, and D. Jiang, "A rate-dependent aging constitutive model of EPDM rubber," *Colloid and Polymer Science,* vol. 302, no. 7, pp. 1037-1052, 2024.

[23] *ANSYS Mechanical 18.1, Mechanical APDL Theory Reference for Detailed Theory and Applications*, 2017.

[24] *Metals Handbook*, A. S. o. Metals, 1998.

[25] S. Buchen, N. H. Kröger, T. Reppel, and K. Weinberg, "Time-dependent modeling and experimental characterization of foamed EPDM rubber," *Continuum Mechanics and Thermodynamics,* vol. 33, no. 4, pp. 1747-1764, 2021.

[26] *Stainless Steel Hex Bolts Recommended Tightning Torque*.

© 2026 by the authors. Creative Commons Attribution (CC BY) license (http://creativecommons.org/licenses/by/4.0/).